Journal of Molecular Catalysis A: Chemical 305 (2009) 147–154

Contents lists available at ScienceDirect

Journal of Molecular Catalysis A: Chemical

journal homepage: www.elsevier.com/locate/molcata

# Effect of key operational parameters on the photocatalytic oxidation of phenol by nanocrystalline sol–gel $TiO_2$ under UV irradiation☆

Cláudia Gomes Silva, Joaquim Luís Faria*

*Laboratório de Catálise e Materiais (LCM), Laboratório Associado LSRE/LCM, Departamento de Engenharia Química, Faculdade de Engenharia, Universidade do Porto, Rua Dr. Roberto Frias, s/n 4200-465 Porto, Portugal*

ARTICLE INFO

*Article history:*
Available online 30 December 2008

*Keywords:*
Heterogeneous photocatalysis
Titanium dioxide
Nanomaterials
Sol–gel catalysts
Kinetics

ABSTRACT

Nanocrystalline $TiO_2$ materials produced by an acid-catalyzed sol–gel method are used as catalysts in the photocatalytic degradation of phenol under ultraviolet light. Materials with different crystalline and morphological properties are obtained by controlling the temperature used in the calcination step. Induced light conversion and adsorption have opposite dependencies on the light intensity. The operational parameters (nature of $TiO_2$ crystal phase, catalyst concentration, pH and initial phenol concentration) have the expected influence in the efficiency of the photocatalytic degradation process. The effect of two different co-oxidants ($H_2O_2$ and $Na_2S_2O_8$) in the photocatalytic process is also described. A modified Langmuir–Hinshelwood kinetic model is used considering a pseudo-steady state approach in order to explain the dependence of both, the kinetic rate and adsorption equilibrium constants, on light intensity. Hydroquinone and catechol are the main intermediates of the photocatalytic reaction, as result from the reaction of phenol with photogenerated hydroxyl radicals. A possible degradation pathway is advanced.


## 1. Introduction

Heterogeneous photocatalysis is nowadays recognized as a strategic area of growing importance in what concerns the development of sustainable technologies for energy production and storage [1], green chemical synthesis [2] and water [3] and air [4] treatment. It can be used together with other techniques for soil remediation [5] and chemical control [6]. The photocatalytic process starts with the irradiation of a semiconductor material by light with sufficient energy to excite the electrons form the valence to the conduction band generating extremely reactive electron/hole ($e^-/h^+$) pairs which migrate to the surface of the semiconductor where they can react with adsorbed species. Positively charged holes react with adsorbed water molecules or hydroxyl anions leading to the formation of the hydroxyl radical, $HO^\bullet$. The surface electrons are transferred to adsorbed oxygen originating the superoxide radical anion, $O_2^{\bullet -}$, which may undergo protonation to the hydroperoxyl radical, $HO_2^\bullet$. Some other adsorbed compounds can react with the surface holes and/or electrons resulting in oxidation and/or reduction products, respectively.

Although radical species like $HO_2^\bullet$ and $O_2^{\bullet -}$ are able to oxidize most of the organic compounds, hydroxyl radical is regarded as the major responsible species for the complete oxidation of organic pollutants [7,8].

Titanium dioxide ($TiO_2$) has been extensively employed as a photocatalyst in wastewater treatment by oxidative degradation [9–12]. The most popular form of this material is the commercially available ready-to-use P 25 from Evonik Degussa, consisting of roughly 75:25 anatase to rutile weight ratio of $TiO_2$. Titanium dioxide can be prepared by both liquid and gas phase processes. For laboratory purposes, the sol–gel method is one of the most used techniques to synthesize films, powders and membranes [13–15]. The sol–gel method has many advantages over other production techniques, including ease of processing, control over the composition, purity and homogeneity of the obtained materials [16].

In the present work nanocrystalline sol–gel $TiO_2$ catalysts were produced, characterized and used in the photocatalytic degradation of phenol under ultraviolet irradiation. Several studies about photooxidation of phenol have already been published [17–19], especially because phenol and phenolic derivatives are commonly found in industrial wastewaters [20–22]. These compounds are normally refractory and recalcitrant limiting the benefits of the preferred biological treatment process. Therefore, phenol is a very useful model pollutant for photocatalytic studies.

Kinetics and mechanism of the photocatalytic oxidation of phenol in a slurry reactor (where the catalyst is suspended in the liquid phase) are here investigated. Besides of being very simple, slurry (or immersion) reactors are very popular, because of the easy handling and inexistence of mass transfer limitations. The major drawback of these reactors relies on the fact that due to geometry diversity,

☆ Paper submitted by occasion of the Symposium in Honor of Eric Derouane.

* Corresponding author. Tel.: +351 225 081 645; fax: +351 225 081 449.
*E-mail address:* jlfaria@fe.up.pt (J.L. Faria).

1381-1169/$ – see front matter © 2008 Elsevier B.V. All rights reserved.
doi:10.1016/j.molcata.2008.12.015

comparisons are difficult to rationalize, therefore limiting their value in establishing reliable models for practical purposes. In addition, real case applications of slurry systems require a final separation step, which complicates the process and increases costs. On the other hand, slurry reactors are more efficient than photocatalytic reactors with immobilized catalysts. In addition, for the present study we use synthesized $TiO_2$ nanoparticles in order to increase the surface to treated volume ratio, therefore aiming to further enhance efficiency.

In order to fully characterize the photocatalytic process, parameters such as $TiO_2$ physical–chemical properties, catalyst loading, pH, phenol concentration, light intensity and presence of added oxidant species are here investigated.

Because modeling photocatalytic reactions requires a tough knowledge of the adsorption phenomena, we present a detailed set of experiments for describing the importance of light-induced adsorption on materials with different anatase to rutile ratio. A pseudo-steady state kinetic approach is used to describe the dependency of the Langmuir–Hinshelwood rate constant, $k_{LH}$, and apparent adsorption constant, $K_{LH}$, on the incident light intensity.

## 2. Experimental

### 2.1. Catalyst preparation and characterization

$TiO_2$ was prepared by an acid-catalyzed sol–gel method from titanium(IV)-isopropoxide (Aldrich 97%) using ethanol as solvent as described elsewhere [15]. The obtained gel was aged in air for 1 week and then ground into a fine powder and dried at room temperature. Finally the powder was calcined in a nitrogen flow for 2 h. Thermal treatment was performed at four calcination temperatures, 400 °C, 500 °C, 550 °C and 700 °C, in order to obtain materials with different properties. The obtained catalysts were labeled as $TiO_2$-A, $TiO_2$-AR, $TiO_2$-RA and $TiO_2$-R, respectively.

Catalysts were characterized by several spectroscopic and micrographic techniques. $N_2$ adsorption–desorption isotherms were measured by using a Coulter Omnisorp 100 CX instrument and the surface area was calculated by the BET method. Powder X-ray diffraction (XRD) patterns were recorded in the range $2\theta = 20$–$60^\circ$ on a Philips X'Pert MPD rotatory target diffractometer, using Cu Ka radiation ($\lambda = 0.15406$ nm) as X-ray source, operated at 40 kV and 100 mA. Anatase to rutile mass ratio was estimated by taking into account the relative integrated intensities of (1 0 1) and (1 1 0) diffraction peaks, respectively [23]. The crystallite dimensions of anatase and rutile crystallites were calculated using Scherrer's equation [24,25]. Transmission electron microscopy (TEM) was performed on a Leica LEO 906E instrument operating at 120 kV. The samples were previously dispersed in ethanol.

### 2.2. Photocatalytic degradation of phenol

Photocatalytic activity was evaluated following the degradation of phenol (PhOH, Aldrich redistilled, 99 + %) in aqueous solution under ultraviolet irradiation. The experiments were carried out in a glass immersion photochemical reactor loaded with 800 ml of suspension. The reactor was equipped with a Heraeus TNN 15/32 low-pressure mercury vapor lamp, with a dominant emission line at 253.7 nm, which was located axially and held in a quartz immersion tube. The intensity of the incident light inside the photoreactor, measured by potassium ferrioxalate actinometry [26], was of $4.78 \times 10^{-6}$ Einstein $s^{-1}$. The photon flow was varied by using a quartz-glass jacket around the light source with dye solutions of different concentrations flowing inside of it.

In a typical experiment, the initial phenol concentration and the amount of suspended $TiO_2$ were set at 50 mg $l^{-1}$ and 1 g $l^{-1}$, respectively. A 200 ml $min^{-1}$ oxygen/argon (20% vol. of oxygen) stream was continuously supplied to the reactor. Before turning on the illumination, the suspensions were saturated with the gas mixture and magnetically stirred for 30 min to establish an adsorption–desorption equilibrium. Then, the suspensions were irradiated with UV light at constant stirring speed.

Samples were regularly withdrawn from the reactor and centrifuged prior to analysis for separation of any suspended solid. The clean transparent solution was then analyzed by HPLC using a Hitachi Elite LaChrom liquid chromatograph equipped with an L-2450 diode array detector. The stationary phase consisted in a Purospher Star RP-18 endcapped column (250 mm × 4.6 mm, 5 μm particles) working at room temperature. The mobile phase was a mixture of water and methanol with a gradient concentration at a flow rate of 1 ml $min^{-1}$. For known compounds, the relationship between area and concentration was determined by using standards. Total organic carbon (TOC) measurements were performed in a Shimadzu TOC-5000 analyzer.

The effect of added co-oxidants was tested using hydrogen peroxide (35 wt.% in $H_2O$, from Sigma–Aldrich) and sodium peroxodisulfate ($Na_2S_2O_8$, purum p.a. ≥99.0%, from Fluka) in the required amounts.

## 3. Results and discussion

Catalyst loading, substrate concentration, pH and photonic flow are found to be crucial parameters in heterogeneous photocatalytic reactions [27]. Preliminary experiments revealed that photocatalytic oxidation of phenol follow a pseudo-first order kinetic model, as described by the following equation:

$$[\mathrm{PhOH}] = [\mathrm{PhOH}]_0 \, e^{-k_{app} t} \quad (1)$$

where [PhOH] corresponds to phenol concentration, $k_{app}$ is the apparent first order kinetic constant, $t$ is the reaction time and $[\mathrm{PhOH}]_0$ is the phenol concentration for $t = 0$ (at the instant that illumination is turned on). Operational parameters were therefore evaluated comparing the values of $k_{app}$, obtained by non-linear regression. Additionally, total organic carbon measurements were performed in order to quantify the mineralization extent.

$TiO_2$ catalysts obtained by sol–gel method at different calcination temperature were tested in the photodegradation of phenol under UV irradiation. Several factors, including surface area, crystal composition and crystal phase contribute to the photocatalytic performance of $TiO_2$ [28,29]. Titania can be found in three crystal forms: anatase, rutile and brookite. Anatase is usually found to be the most photocatalytically active crystal phase [30].

Catalysts characterization is summarized in Table 1. XRD data (shown as Supplementary material) revealed that the catalyst obtained at 400 °C ($TiO_2$-A) consists in pure anatase. Higher temperature promotes the transformation of anatase to $TiO_2$ more stable polymorph, rutile. Anatase to rutile transition occurs at temperature between 400 °C and 500 °C. $TiO_2$-AR and $TiO_2$-RA are mixtures of anatase and rutile crystalline phases with 69% and 38% of anatase, respectively. At 700 °C the catalyst is constituted by pure rutile.

As calcination temperature increases, crystallites tend to agglomerate originating bigger crystal particles with the

**Table 1**
Anatase (A) and rutile (R) crystallite dimensions ($d$), surface area ($S$) and crystal composition of $TiO_2$ catalysts obtained with different temperature ($T_c$).

| Catalyst | $T_c$ (°C) | $d_A$ (nm) | $d_R$ (nm) | $S$ ($m^2$ $g^{-1}$) | Crystal composition |
|---|---|---|---|---|---|
| $TiO_2$-A | 400 | 8.5 | – | 107 | 100% A |
| $TiO_2$-AR | 500 | 14 | 20 | 26 | 69% A + 31% R |
| $TiO_2$-RA | 550 | 23 | 24 | 13 | 38% A + 62% R |
| $TiO_2$-R | 700 | – | 39 | 3 | 100% R |

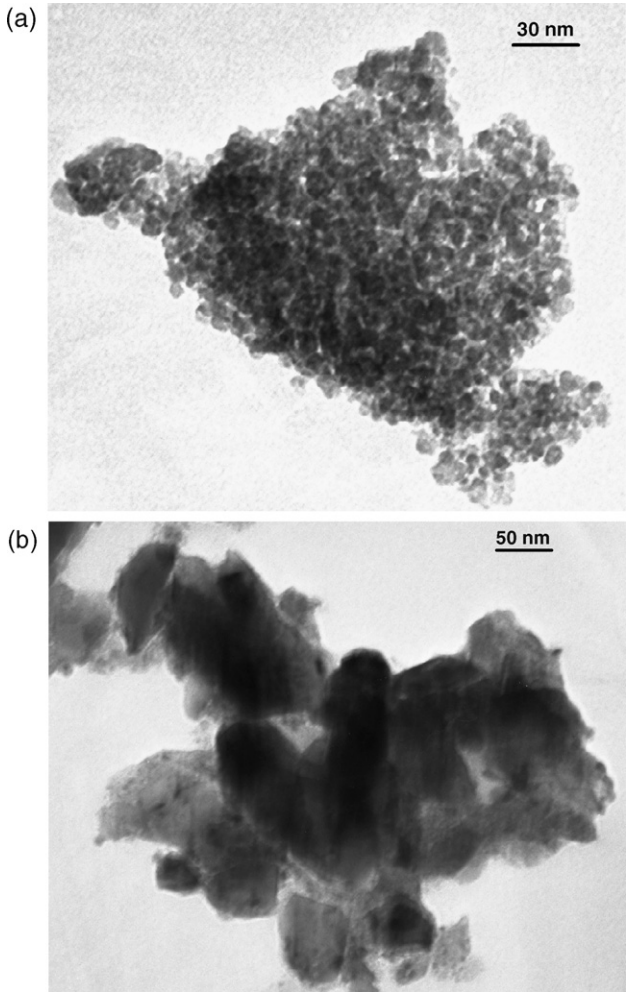


**Fig. 1.** TEM micrographs of (a) $TiO_2$-A and (b) $TiO_2$-R.

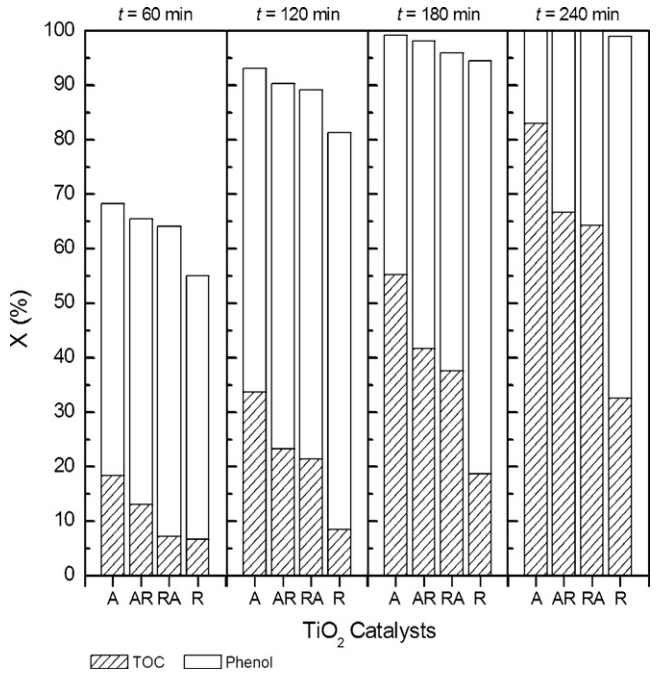


**Fig. 2.** Total organic carbon removal (%) and carbon contained in phenol removal (%) during photodegradation experiments with different catalysts.

subsequent decreasing in the surface area of the solids. TEM micrographs of $TiO_2$-A and $TiO_2$-R are shown in Fig. 1a and b, respectively. Crystallite with dimensions similar to the calculated by XRD data could be observed.

In a typical experiment phenol solutions were subjected to UV irradiation for 4 h. In all cases, the total conversion of phenol was achieved at the end of the reaction. $TiO_2$-A showed the best catalytic activity. A decrease in the apparent kinetic rate constant with the decrease in the anatase content was observed. Apparent kinetic rate constants, determined by non-linear curve fitting, were found to be of $2.04 \times 10^{-2}$ min$^{-1}$, $1.83 \times 10^{-2}$ min$^{-1}$, $1.82 \times 10^{-2}$ min$^{-1}$ and $1.42 \times 10^{-2}$ min$^{-1}$ for $TiO_2$-A, $TiO_2$-AR, $TiO_2$-RA and $TiO_2$-R, respectively. The same tendency was observed for total organic carbon removal. After four (4) h of irradiation, reaction using $TiO_2$-A as catalyst resulted in 83% TOC reduction, while $TiO_2$-AR, $TiO_2$-RA and $TiO_2$-R could only remove 66%, 64% and 33%, respectively. As can be observed in Fig. 2, phenol was totally converted at the end of the photodegradation reaction. Nevertheless, there is still a fraction of non-mineralized organic compounds, probably corresponding to aliphatic acids, not detected by HPLC, such as lactic, acetic, formic, maleic, oxalic and others resulting from the aromatic ring opening [31,32] and contributing to the carbon content remaining in solution.

For comparison purposes, commercial $TiO_2$ Degussa P25, consisting of a mixture of 75% anatase and 25% rutile phase with a surface area of 50 m$^2$ g$^{-1}$, was used in the photocatalytic degradation of phenol under UV irradiation in similar conditions. In this case, the first order kinetic rate constant was of $1.72 \times 10^{-2}$ min$^{-1}$, with a 97% of TOC reduction after 4 h of irradiation.

It was found that $TiO_2$ photocatalytic efficiency decreases with increasing calcination temperature. $TiO_2$-A was found to be the most active catalyst for the photodecomposition of phenol under UV light. The deterioration of photocatalysis efficiency is attributed to the phase transformation from anatase to rutile as well as particle segregation after calcination at higher temperature. Thus, $TiO_2$-A was used as catalyst in order to optimize key parameters of the photodegradation of phenol under UV light.

### 3.1. Effect of catalyst load

In order to avoid an ineffective excess of catalyst and to ensure a total absorption of efficient photons, the optimum mass of catalyst needs to be found. In this study, $TiO_2$-A concentration in the suspension was varied from 0.10 to 1.5 g l$^{-1}$. As shown in Table 2, $k_{app}$ increased with the mass of catalyst up to an amount of 1 g l$^{-1}$, confirming the heterogeneous nature of the photocatalytic process. This behavior can be associated to an increment of the active sites available for phenol adsorption and degradation. However, an increase on the catalyst loading to 1.5 g l$^{-1}$ resulted in a decrease in the apparent rate constant, which can be attributed to a screening effect due to the redundant dispersion of UV radiation caused by the substantial amount of suspended photocatalyst. Furthermore, in these conditions, particles tend to agglomerate, making a significant fraction of the catalyst to be inaccessible to either adsorbing

**Table 2**
Apparent first-order kinetic rate constants and TOC removal after 4 h of irradiation obtained for different $TiO_2$ concentrations.

| $C_{TiO_2}$ (g l$^{-1}$) | $k_{app}$ ($\times 10^{-2}$ min$^{-1}$) | $X_{TOC,4h}$ (%) |
|---|---|---|
| 0.10 | 1.52 ± 0.07 | 29 |
| 0.20 | 1.56 ± 0.07 | 32 |
| 0.50 | 1.74 ± 0.06 | 44 |
| 1.0 | 2.04 ± 0.05 | 83 |
| 1.5 | 1.91 ± 0.04 | 76 |

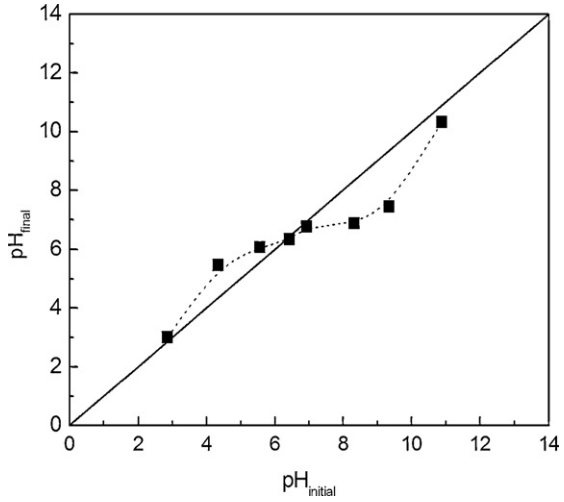


**Fig. 3.** Determination of the point of zero charge of $TiO_2$-A.

the molecules or absorbing the radiation, with consequent decrease in the active sites available to the catalytic reaction.

Following these observations, it was decided to keep the amount of $TiO_2$ at the optimum value of 1 g $l^{-1}$ in subsequent photocatalytic degradation experiments.

### 3.2. Effect of pH

As expected $TiO_2$ shows amphoteric behavior in aqueous media. The point of zero charge (pzc) of $TiO_2$-A, *i.e.* the point when the surface charge density is zero, determined by the procedure indicated in Ref. [33], was found to be of 6.4, as shown in Fig. 3 (the pH at which the curve crosses the line $pH_{initial} = pH_{final}$ is taken as the point of zero charge, $pH_{pzc}$). At pH higher than $pH_{pzc}$, $TiO_2$ surface is negatively charged and $TiO^-$ appears to be the predominant form. For lower pH values, titania surface is in the protonated form ($TiOH_2^+$). Electric charge properties of both, catalyst and substrate, are found to play an important role on adsorption process. Under aqueous media, phenol shows a pKa of 9.9 (at 25 °C), which means that for $pH < pK_a$, it is in the molecular form ($C_6H_5OH$) and at $pH > pK_a$ the molecule undergoes deprotonation becoming negatively charged ($C_6H_5O^-$).

The pH of the suspensions was varied in order to study its effect in the photocatalytic degradation of phenol. As can be seen in Fig. 4, basically no effect was observed when pH was decreased from 5 (natural pH) to 3.

Apparent first order kinetic rate constants were found to be of $2.04 \times 10^{-2}$ $min^{-1}$ and $2.06 \times 10^{-2}$ $min^{-1}$, respectively. However, at pH 11, the photoefficiency of the process drastically decreases, and phenol removal becomes very slow, with a $k_{app}$ of $4.70 \times 10^{-3}$ $min^{-1}$. Under these conditions, both catalyst and substrate are negatively charged, developing repulsive forces between them, thus decreasing substrate adsorption.

### 3.3. Effect of photonic flow

In order to study the influence of different light intensity in the photocatalytic degradation of phenol, a quartz jacket was placed around the irradiation source and inside of it a dye (C.I. Direct Green 26, $\varepsilon_{254nm} = 32346\ M^{-1}\ cm^{-1}$) solution was circulating, acting as a light filter. Solutions of the dye with different concentrations were used in order to filter different fractions of light. Radiation intensities were determined by ferrioxalate actinometry and are here presented as fractions of the initial flow ($\varphi/\varphi_0$), *i.e.*, the photonic flow obtained when water is passing throw the quartz jacket. For the range of intensities studied, the apparent rate constant revealed to change linearly with the photonic flow (Fig. 5), which confirms the photo-induced nature of the catalytic process.

It is known that for high photonic flows, the instantaneous rate of formation of $e^-/h^+$ pairs become higher than photocatalytic reaction rate ($r$) and $r$ become proportional to $\varphi^{1/2}$ [34]. Nevertheless, it is also known that the optimum light power utilization corresponds to the domain where $r$ is proportional to $\varphi$ [27].

The effect of light intensity on the adsorption of phenol and kinetics its conversion are further detailed in Section 3.5.

### 3.4. Effect of oxidant species

Photocatalytic reaction major energy wasting step consists in the recombination of photogenerated electrons and holes leading to the low quantum yield of the process. Electron-hole recombination can be prevented by adding a proper electron acceptor to the system. Generally molecular oxygen, pure or in air, is used for this purpose. In order to compensate for the lack of oxygen caused either by consumption or slow oxygen mass transfer, the addition of inorganic oxidants to the semiconductor suspension such as $H_2O_2$, $KClO_3$, $Na_2S_2O_8$, $KBrO_3$ and $KIO_4$ must be considered [35–37]. These compounds show a positive effect on the rate of the photocatalytic

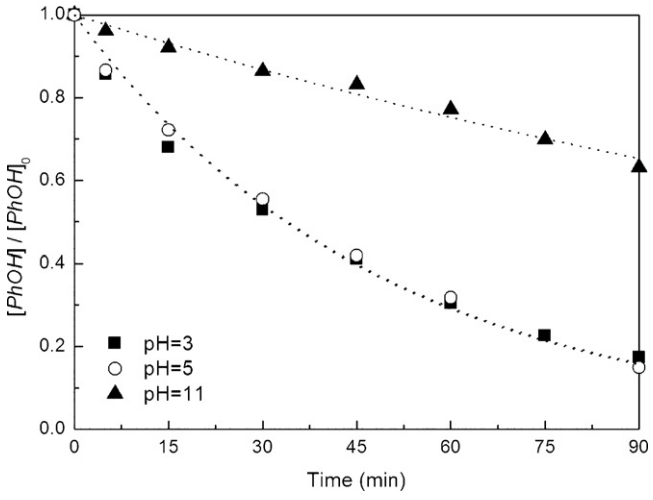


**Fig. 4.** Effect of pH on phenol photocatalytic oxidation.

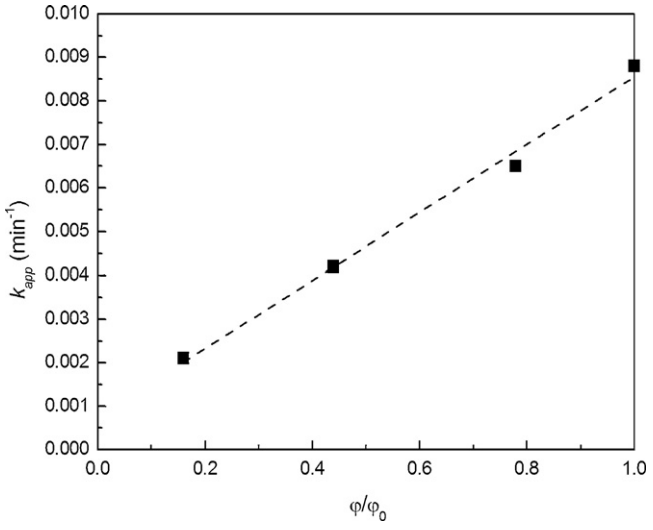


**Fig. 5.** Apparent rate constant as function of the photonic flow.

oxidation of organic molecules in water by avoiding electron/hole recombination, as they act as electron acceptors. In the present study, hydrogen peroxide and sodium peroxodisulfate were tested as oxidants in the photocatalytic oxidation of phenol.

Hydrogen peroxide plays a dual role in photocatalytic reaction acting as electron acceptor, promoting the charge separation, being also able to decompose to produce HO• radicals by absorption of light at 254 nm:

$$H_2O_2 + e_{cb}^- \rightarrow HO^\bullet + HO^- \quad (2)$$

$$H_2O_2 \xrightarrow{h\upsilon} 2HO^\bullet \quad (3)$$

Hydroxyl radicals can as well be produced by reaction of $H_2O_2$ with superoxide radical anion as follows:

$$H_2O_2 + O_2^{\bullet -} \rightarrow HO^\bullet + HO^- + O_2 \quad (4)$$

The addition of $H_2O_2$ to $TiO_2$ suspensions resulted in a significant increase on the kinetics of phenol photo-degradation (Fig. 6). Total removal of phenol was observed at an irradiation time of less than 60 min. At that time, a 58% TOC removal was achieved and at the end of 4 h of irradiation a 93% TOC decrease was observed, meaning a close to total mineralization.

The introduction of peroxodisulfate anion also produced a beneficial effect on phenol degradation rate (Fig. 6). This positive effect is not only attributed to the promotion of semiconductor charge separation by reacting with conduction band electrons but also to the production of extremely oxidizing ($E^0 = 2.6$ eV) sulfate radicals capable of react with most organic molecules:

$$S_2O_8^{2-} \xrightarrow{h\upsilon} 2SO_4^{\bullet -} \quad (5)$$

$$S_2O_8^{2-} + e_{cb}^- \rightarrow SO_4^{\bullet -} + SO_4^{2-} \quad (6)$$

$$SO_4^{\bullet -} + e_{cb}^- \rightarrow SO_4^{2-} \quad (7)$$

$$SO_4^{\bullet -} + H_2O \rightarrow HO^\bullet + SO_4^{2-} + H^+ \quad (8)$$

$$SO_4^{\bullet -} + R \rightarrow SO_4^{2-} + \text{intermediates} \quad (9)$$

At the end of 1 h of irradiation total removal of phenol was reached with a TOC reduction of 59% being of 94% at the end of 4 h of irradiation.

### 3.5. Phenol concentration—kinetics of conversion

The initial phenol concentration (before dark adsorption) was varied from 10 to 50 mg $l^{-1}$. Results showed that for this range of concentrations the reaction rate gets slower as the initial concentration of phenol in solution increases (Fig. 7). The first-order apparent rate constant obtained for the reaction with the 10 mg $l^{-1}$ phenol solution was of $9.32 \times 10^{-2}$ $min^{-1}$ while for the higher initial concentration (50 mg $l^{-1}$) a $k_{app}$ of $2.04 \times 10^{-2}$ $min^{-1}$ was obtained. As phenol concentration increases, more reactant and reaction intermediates are adsorbed on the surface of the photocatalyst, therefore, the generation of hydroxyl radicals will be reduced since are only a fewer active sites for adsorption of hydroxyl anions.

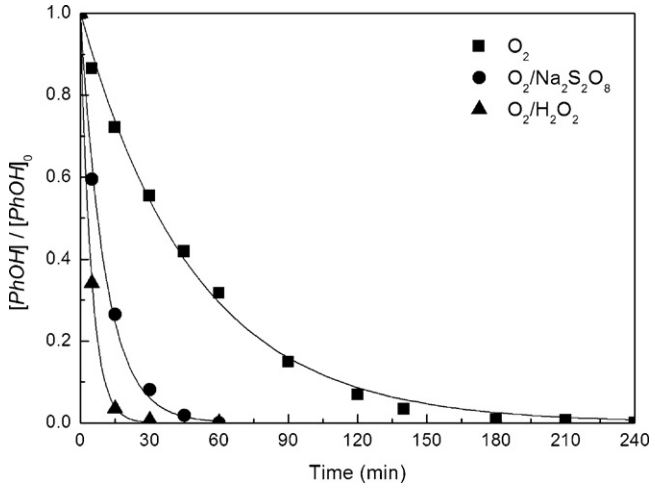


**Fig. 6.** Effect of oxidants on photocatalytic degradation of phenol.

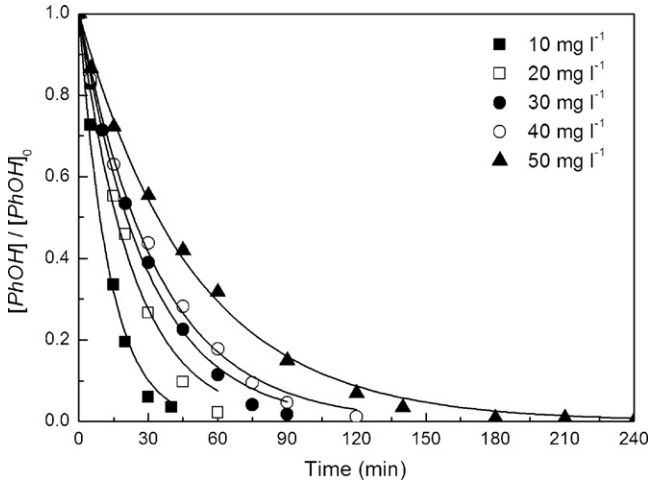


**Fig. 7.** Effect of the initial concentration of phenol on the kinetics of the photocatalytic reaction.

The dependency of the photocatalytic reaction rate on the concentration of the organic substrate has been generally well described by a Langmuir–Hinshelwood kinetic model [27]:

$$-r_A = k_{LH} \frac{K_{LH} C_A}{1 + K_{LH} C_A} \quad (10)$$

where $r_A$ is the rate of degradation of the organic compound A, and $k_{LH}$ and $K_{LH}$ are the apparent reaction rate and the apparent Langmuir adsorption constants, respectively.

The reaction mechanism usually considered for heterogeneous photocatalyzed reactions consist in two main steps: fast adsorption of the reactants on the catalyst surface Eq. (11) and a slow step of reaction in the adsorbed phase of the organic compound and a photogenerated hydroxyl radical Eq. (12), as follows:

$$A \underset{k_{-1}}{\overset{k_1}{\rightleftarrows}} A_{ads} \quad (11)$$

$$A_{ads} \xrightarrow{k_{LH}} products \quad (12)$$

Although this is well established and greatly used for most of the authors to describe the kinetics of photo-oxidation reactions, some considerations have to be taking into account. It has been recognized that $k_{LH}$ and $K_{LH}$ are light intensity-dependent [38–41]. $K_{LH}$ in a photocatalytic oxidation reaction has not the same meaning as the $K_{ads}$ dark adsorption constant. In photo-induced reactions, the number of active catalyst sites is much fewer than the total surface adsorption sites. Thus, the $K_{LH}$ value measured under illumination does not characterize the generally accessible surface probed by dark adsorption measurements. Another fact is that the active sites exist only under illumination and the species involved do not exist appreciably in the dark. Additionally, the determining rate step Eq. (12) involves the reaction of the adsorbed substrate with a photogenerated HO• radical. Since the latter will be a function of absorbed light intensity, which in turn will be proportional to the incident light intensity ($I$), it follows that $k_{LH}$ will also be a function

of absorbed light intensity:

$$k_{LH} = \alpha\ I^{\beta} \tag{13}$$

where $\alpha$ is a proportionality constant and $\beta$ is equal to 1.0 or 0.5 at low and high absorbed light intensities, respectively. A pseudo-steady state approach has recently been proposed [39–42] introducing the previously mentioned considerations. Therefore, the surface coverage of the organic compound ($\theta_A$) is given by

$$\theta_A = \frac{K_{LH}C_A}{1 + K_{LH}C_A} \tag{14}$$

with

$$K_{LH} = \frac{1}{K_{LH,diss}} = \frac{k_1}{k_{-1} + \alpha I^{\beta}} \tag{15}$$

and $K_{LH,diss}$ being the apparent dissociation constant.

Thus, the general intensity dependence of the photocatalyzed reaction is given by

$$-r_A = k_{LH}\theta_A = \frac{k_{LH}C_A}{k_{LH,diss} + C_A} \tag{16}$$

This pseudo-steady state approach predicts that both $k_{LH}$ and $K_{LH,diss}$ depend on the intensity of absorbed light [40]. In this study, $k_{LH}$ and $K_{LH}$ constants were determined for two light intensities correspondent to a photon flow of $4.78 \times 10^{-6}$ and $2.05 \times 10^{-6}$ Einstein $s^{-1}$ (Table 3).

Results showed that $k_{LH}$ is proportional to the photon flow while $K_{LH}$ decreased for higher light intensity. As photon flow increases, the number of photogenerated HO• radicals rise up accelerating the oxidation of the substrate molecules. Simultaneously, the increase of surface active species such as electrons, holes and HO• radicals lead to a decrease in the available sites for adsorption of the primary molecule and therefore a decrease in $K_{LH}$.

### 3.6. Product analysis and reaction mechanism

HPLC analysis performed during the photocatalytic runs revealed that, despite the catalyst used, the primary reaction intermediates are single-substituted hydroxyl derivates, indicating that HO• radicals are the key species involved in the oxidation process. Catechol (CT; 2-hydroxyphenol) and hydroquinone (HQ; 4-hydroxyphenol) were detected as main intermediates, which is in agreement with the orientating properties of phenol's hydroxyl group. Photocatalytic oxidation of benzene-substituted substrates containing electron donor groups, such as phenol, generate *ortho* and *para* hydroxy derivatives as primary intermediates [43]. Trace concentrations of benzoquinone (in equilibrium with hydroquinone) were also detected. Therefore, a simplified reaction mechanism is proposed (Scheme 1).

A kinetic model was developed taking into account the following observations: (i) phenol concentration decays following a pseudo-first order rate law, reaching at the end of the photocatalytic run essentially zero concentration; (ii) The concentration of the main reaction intermediates initially rise and then decrease until almost complete disappearance at the same time of complete phenol conversion. Assuming all reactions to be first order, the rate expression of phenol, catechol (CT) and hydroquinone (HQ) can be expressed as follows:

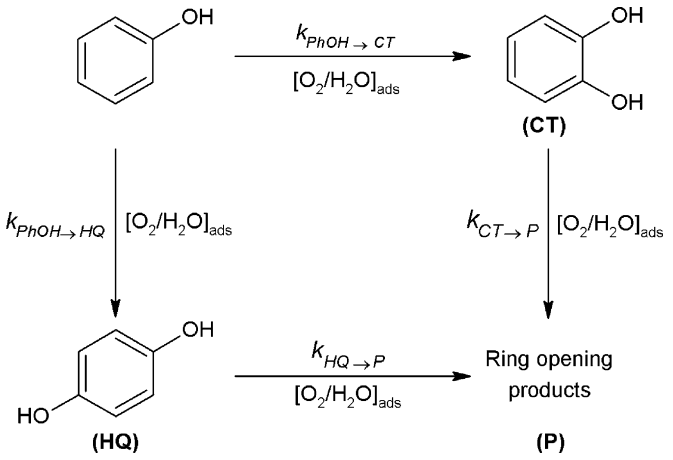


**Scheme 1.**

$$\frac{d[\mathrm{PhOH}]}{dt} = -(k_{\mathrm{PhOH}\rightarrow\mathrm{CT}} + k_{\mathrm{PhOH}\rightarrow\mathrm{HQ}})[\mathrm{PhOH}] \tag{17}$$

$$\frac{d[\mathrm{CT}]}{dt} = k_{\mathrm{PhOH}\rightarrow\mathrm{CT}}[\mathrm{PhOH}] - k_{\mathrm{CT}\rightarrow\mathrm{P}}[\mathrm{CT}] \tag{18}$$

$$\frac{d[\mathrm{HQ}]}{dt} = k_{\mathrm{PhOH}\rightarrow\mathrm{HQ}}[\mathrm{PhOH}] - k_{\mathrm{HQ}\rightarrow\mathrm{P}}[\mathrm{HQ}] \tag{19}$$

being $k_{\mathrm{PhOH}\rightarrow\mathrm{CT}}$, $k_{\mathrm{PhOH}\rightarrow\mathrm{HQ}}$, $k_{\mathrm{CT}\rightarrow\mathrm{P}}$ and $k_{\mathrm{HQ}\rightarrow\mathrm{P}}$ the first order apparent rate constants for the formation and consumption of phenol, catechol and hydroquinone as represented in Scheme 1.

The linear first order ODEs were solved using MatLab and non-linearly regressed with experimental data to obtain the kinetic rate constants (Table 4).

The rate of photocatalytic removal for phenol ($k_{\mathrm{PhOH}\rightarrow\mathrm{CT}} + k_{\mathrm{PhOH}\rightarrow\mathrm{HQ}}$) follows the order $TiO_2$-A > $TiO_2$-AR > $TiO_2$-RA > $TiO_2$-R, which is agreement with our previous observations. In fact ($k_{\mathrm{PhOH}\rightarrow\mathrm{CT}} + k_{\mathrm{PhOH}\rightarrow\mathrm{HQ}}$) values correspond almost exactly to the values of $k_{app}$ obtained by non-linear curve fitting of the phenol decay experimental data to Eq. (1). Concentration profiles (experimental and model fit) for phenol, catechol and hydroquinone obtained during the photocatalytic oxidation reactions using $TiO_2$-A and $TiO_2$-R are shown in Fig. 8a and b, respectively.

As rutile fraction increases, phenol, catechol and hydroquinone formation and disappearance rate constants tend to decrease as a result of the loss of activity of the photocatalysts. Although $TiO_2$-AR and $TiO_2$-RA show similar $k_{\mathrm{PhOH}\rightarrow\mathrm{CT}}$ and $k_{\mathrm{PhOH}\rightarrow\mathrm{HQ}}$ values, *i e.*, similar efficiency on the removal of phenol, a decrease in $k_{\mathrm{CT}\rightarrow\mathrm{P}}$ and $k_{\mathrm{HQ}\rightarrow\mathrm{P}}$ for $TiO_2$-RA catalyst is observed. The higher percentage of rutile phase and higher crystal particle dimension contribute both for the decrease on the photoefficiency of the catalyst, inhibiting the formation of HO• radicals and slowing down the degradation of the intermediate species.

The model fit well the experimental data confirming the validity of the proposed reaction mechanism.

**Table 3**
Langmuir–Hinshelwood parameters, $k_{LH}$ and $K_{LH}$ as a function of the photonic flow ($\varphi$).

| $\varphi$ ($\times 10^{-6}$ Einstein $s^{-1}$) | $k_{LH}$ ($\times 10^{-5}$ M $min^{-1}$) | $K_{LH}$ ($\times 10^{4}$ $M^{-1}$) |
|---|---|---|
| 4.78 | 1.10 | 1.520 |
| 2.05 | 0.55 | 2.825 |

**Table 4**
First order apparent rate constants, $k$ ($\times 10^{-2}$ $min^{-1}$), for the photocatalytic oxidation of phenol using different $TiO_2$ catalysts.

| Catalyst | $k_{\mathrm{PhOH}\rightarrow\mathrm{CT}}$ | $k_{\mathrm{PhOH}\rightarrow\mathrm{HQ}}$ | $k_{\mathrm{CT}\rightarrow\mathrm{P}}$ | $k_{\mathrm{HQ}\rightarrow\mathrm{P}}$ | $k_{app}$ |
|---|---|---|---|---|---|
| $TiO_2$-A | 1.29 | 0.72 | 1.58 | 2.27 | 2.04 |
| $TiO_2$-AR | 1.28 | 0.60 | 1.23 | 1.33 | 1.83 |
| $TiO_2$-RA | 1.27 | 0.59 | 1.15 | 1.24 | 1.82 |
| $TiO_2$-R | 0.97 | 0.45 | 0.89 | 1.03 | 1.42 |

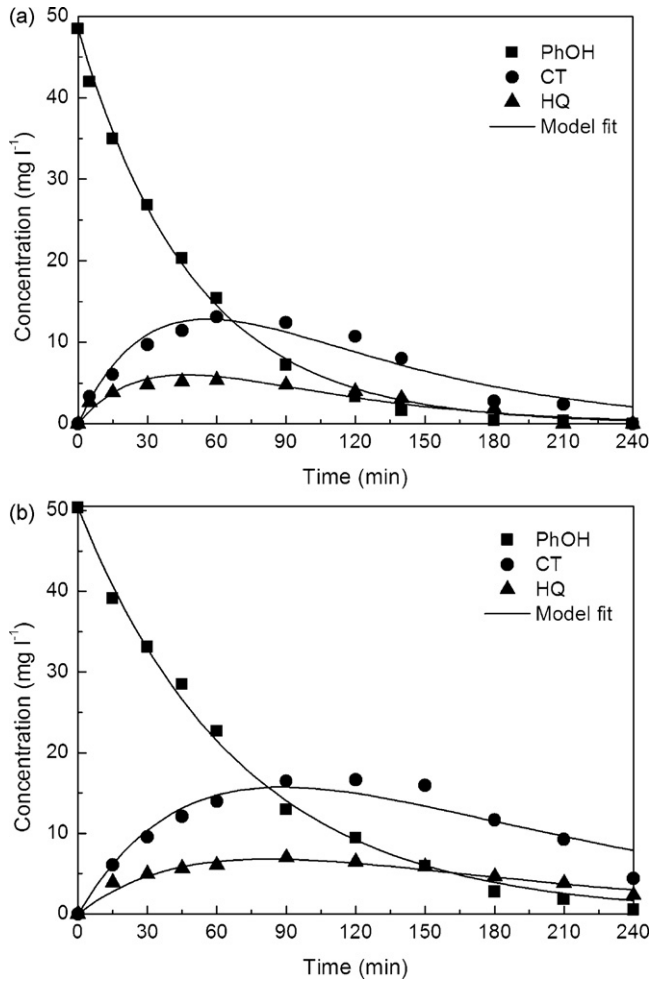


**Fig. 8.** Concentration profiles of PhOH, CT and HQ and model fit for the photocatalytic degradation of phenol using $TiO_2$-A (a) and $TiO_2$-R (b) as catalyst.

## 4. Conclusions

Acid catalyzed sol–gel method can be successfully used to produce $TiO_2$ nanoparticles with different ratios of anatase to rutile crystal phases. Within the preparation method, as the calcination temperature increases, anatase to rutile phase transition occurs and crystallites tend to agglomerate with concomitant loss of activity of the catalyst. Pure anatase $TiO_2$ is found to be more active than rutile in the photocatalytic oxidation of phenol.

The photocatalytic process is influenced by several operating factors such as catalyst loading, initial phenol concentration, pH of the medium, irradiation intensity and presence of oxidant species. The introduction of an added oxidant produces a moderate increase in the oxidation rate, which seems not to depend markedly on the nature of the oxidant. This suggests that the oxidation process is mainly driven from the $HO^{\bullet}$ adsorbed radicals generated from the surface positive holes.

A pseudo-steady state approach applied to the Langmuir–Hinshelwood model is used to explain the dependency of the kinetics on the initial concentration of substrate and on illumination intensity. As photon flow increase, an increase in the kinetic rate constant is observed with a decrease on the adsorption rate constant. This evidences the inhibition effect produced by photodessorption of the organic substrate from the surface of the catalyst. This is in line with the fact that the reaction is essentially a surface reaction between the surface generated oxidative radicals and adsorbed organic substrates.

Hydroquinone and catechol are detected as the main intermediates resulting form the attack of hydroxyl radical in the *para* and *ortho* positions of phenol molecule, respectively. Kinetics of consumption and formation reactions of substrate and intermediates fit well a first order rate law. Apparent kinetic rate constants obtained by solving differential equations and regressing it with experimental data follows the order $TiO_2$-A > $TiO_2$-AR > $TiO_2$-RA > $TiO_2$-R, confirming the influence of the nature of the catalysts in the kinetics of the photocatalytic process.

## Acknowledgments

This research was carried out by projects SFRH/BD/16966/2004, POCI/EQU/58252/2004, POCTI/1181/2003, approved by the FCT, Programa Operacional (POCTI/POCI) and co-supported by FEDER. We would like to thank Dr. Pedro Tavares (UTAD, Portugal) for technical assistance and advice with TEM measurements.

## Appendix A. Supplementary data

Supplementary data associated with this article can be found, in the online version, at doi:10.1016/j.molcata.2008.12.015.

## References

[1] T.-V. Nguyen, H.-C. Lee, O.B. Yang, Sol. Energy Mater. Sol. Cells 90 (2006) 967–981.
[2] H. Park, W. Choi, Catal. Today 101 (2005) 291–297.
[3] D.S. Bhatkhande, V.G. Pangarkar, A.A.C.M. Beenackers, J. Chem. Technol. Biotechnol. 77 (2002) 102–116.
[4] G.P. Zanini, G.A. Arguello, J. Mol. Catal. A: Chem. 159 (2000) 347–351.
[5] M.M. Higarashi, W.F. Jardim, Catal. Today 76 (2002) 201–207.
[6] X. Quan, H. Shi, Y. Zhang, J. Wang, Y. Qian, Sep. Purif. Technol. 34 (2004) 97–103.
[7] Y. Nosaka, Y. Yamashita, H. Fukuyama, J. Phys. Chem. B 101 (1997) 5822–5827.
[8] P.F. Schwarz, N.J. Turro, S.H. Bossmann, A.M. Braun, A. Wahab, H. Durr, J. Phys. Chem. B 101 (1997) 7127–7134.
[9] C.G. da Silva, J.L. Faria, J. Photochem. Photobiol. A: Chem. 155 (2003) 133–143.
[10] O.K. Dalrymple, D.H. Yeh, M.A. Trotz, J. Chem. Technol. Biotechnol. 82 (2007) 121–134.
[11] R. Comparelli, E. Fanizza, M.L. Curri, P.D. Cozzoli, G. Mascolo, R. Passino, A. Agostiano, Appl. Catal. B 55 (2005) 81–91.
[12] C.G. Silva, W.D. Wang, J.L. Faria, J. Photochem. Photobiol. A: Chem. 181 (2006) 314–324.
[13] N. Agoudjil, T. Benkacem, Desalination 206 (2007) 531–537.
[14] N. Kitazawa, H. Sato, Y. Watanabe, J. Mater. Sci. 42 (2007) 5074–5079.
[15] W.D. Wang, C.G. Silva, J.L. Faria, Appl. Catal. B: Environ. 70 (2007) 470–478.
[16] M. Keshmiri, M. Mohseni, T. Troczynski, Appl. Catal. B: Environ. 53 (2004) 209–219.
[17] H. Chun, W. Yizhong, T. Hongxiao, Chemosphere 41 (2000) 1205–1209.
[18] Z. Guo, R. Ma, G. Li, Chem. Eng. J. 119 (2006) 55–59.
[19] A. Sobczynski, L. Duczmal, W. Zmudzinski, J. Mol. Catal. A: Chem. 213 (2004) 225–230.
[20] W. Gernjak, M.I. Maldonado, S. Malato, J. Caceres, T. Krutzler, A. Glaser, R. Bauer, Sol. Energy 77 (2004) 567–572.
[21] M.C. Yeber, J. Rodriguez, J. Freer, N. Duran, H.D. Mansilla, Chemosphere 41 (2000) 1193–1197.
[22] H.T. Gomes, J.L. Figueiredo, J.L. Faria, Catal. Today 124 (2007) 254–259.
[23] R.A. Spurr, H. Myers, Anal. Chem. 29 (1957) 760–762.
[24] H. Natter, M. Schmelzer, M.-S. Löffler, C.E. Krill, A. Fitch, R. Hempelmann, J. Phys. Chem. B 104 (2000) 2467–2476.
[25] Y. Xie, C. Yuan, Appl. Catal. B: Environ. 46 (2003) 251–259.
[26] H.J. Kuhn, S.E. Braslavsky, R. Schmidt, Pure Appl. Chem. 76 (2004) 2105–2146.
[27] J.M. Herrmann, Top. Catal. 34 (2005) 49–65.
[28] G. Colon, J.M. Sanchez-Espana, M.C. Hidalgo, J.A. Navio, J. Photochem. Photobiol. A: Chem. 179 (2006) 20–27.
[29] R.J. Tayade, R.G. Kulkarni, R.V. Jasra, Ind. Eng. Chem. Res. 45 (2006) 922–927.
[30] A. Sclafani, J.M. Herrmann, J. Phys. Chem. 100 (1996) 13655–13661.
[31] B. Tryba, A.W. Morawski, M. Inagaki, M. Toyoda, Appl. Catal. B: Environ. 63 (2006) 215–221.
[32] Z. Wang, W. Cai, X. Hong, X. Zhao, F. Xu, C. Cai, Appl. Catal. B: Environ. 57 (2005) 223–231.
[33] J. Rivera-Utrilla, I. Bautista-Toledo, M.A. Ferro-Garcia, C. Moreno-Castilla, J. Chem. Technol. Biotechnol. 76 (2001) 1209–1215.
[34] A. Mills, J. Wang, D.F. Ollis, J. Catal. 243 (2006) 1–6.
[35] M. Kositzi, A. Antoniadis, I. Poulios, I. Kiridis, S. Malato, Sol. Energy 77 (2004) 591–600.
[36] L. Ravichandran, K. Selvam, M. Swaminathan, Sep. Purif. Technol. 56 (2007) 192–198.

[37] A.M.T. Silva, E. Nouli, N.P. Xekoukoulotakis, D. Mantzavinos, Appl. Catal. B: Environ. 73 (2007) 11–22.
[38] A.V. Emeline, V. Ryabchuk, N. Serpone, J. Photochem. Photobiol. A: Chem. 133 (2000) 89–97.
[39] A. Mills, J. Wang, D.F. Ollis, J. Phys. Chem. B 110 (2006) 14386–14390.
[40] D.F. Ollis, J. Phys. Chem. B 109 (2005) 2439–2444.
[41] D.F. Ollis, Top. Catal. 35 (2005) 217–223.
[42] S. Brosillon, L. Lhomme, C. Vallet, A. Bouzaza, D. Wolbert, Appl. Catal. B: Environ. 78 (2008) 232–241.
[43] G. Palmisano, M. Addamo, V. Augugliaro, T. Caronna, A.D. Paola, E.G. López, V. Loddo, G. Marcì, L. Palmisano, M. Schiavello, Catal. Today 122 (2007) 118–127.